Journal of Materials Chemistry C

Accepted Manuscript

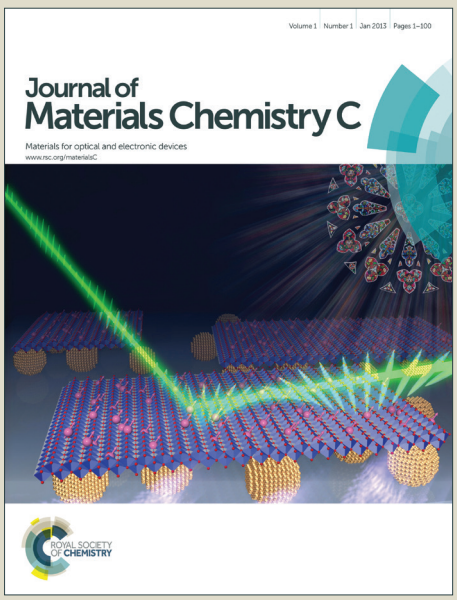

ROYAL SOCIETY OF CHEMISTRY

www.rsc.org/materialsC

Graphical Abstract

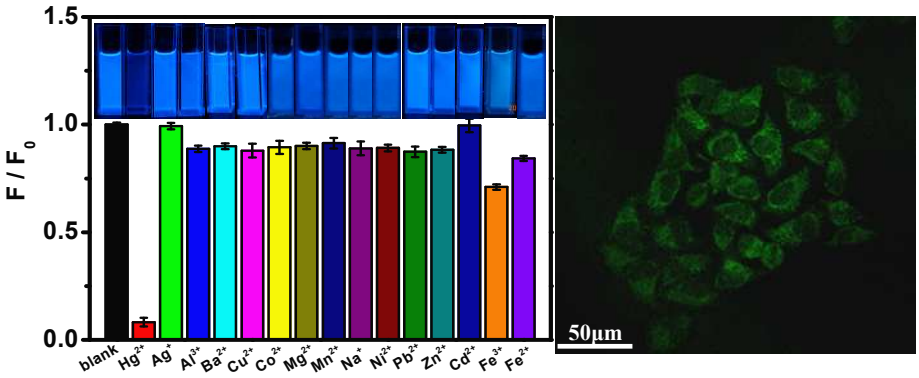

We developed a facile one-step route for facile synthesis of OS-GCNQDs from citric acid and thiourea. The as-prepared OS-GCNQDs showed bright blue photoluminescence, which exhibited improved selectivity and sensitivity for Hg^{2+} detection, along with enhanced biocompatibility and lower cytotoxicity for cell imaging.

Facile synthesis of oxygen and sulfur co-doped graphitic carbon nitride fluorescent quantum dots and their application for mercury (II) detection and bioimaging

Ya-Chun Lu,[a †] Jia Chen,[a †] Ai-Jun Wang,[a] Ning Bao,[b] Jiu-Ju Feng,[a*] Weiping Wang,[a] Linxiang Shao[a*]

[a] *College of Chemistry and Life Science, College of Geography and Environmental Science, Zhejiang Normal University, Jinhua 321004, China*

[b] *School of Public Health, Nantong University, Nantong 226019, China*

**Corresponding author: Tel./Fax: +86-579-82282269, jjfeng@zjnu.cn (JJF); shaolinxiang@zjnu.cn (LXS).*

[†] *These authors contributed equally to this work.*

Abstract

In this work, uniform oxygen and sulfur co-doped graphitic carbon nitride quantum dots (OS-GCNQDs) were prepared by thermal treatment of citric acid and thiourea. The as-obtained OS-GCNQDs show strong blue photoluminescence (PL) with a relatively high quantum yield of 14.5%. Furthermore, OS-GCNQDs exhibit stable and specific concentration-dependent PL intensities in the presence of mercury (II) ions in the range of 0.001 ~ 20.0 μM, with the detection limit at 0.37 nM (3S/N). More importantly, OS-GCNQDs were explored for cell imaging with satisfactory biocompatibility, which are a potential fluorescent probe in biosensing and bioimaging applications.

Keywords: Graphitic carbon nitride; Quantum dots; Fluorescent; Mercury; Bioimaging

Introduction

Carbon quantum dots (CQDs) have received growing research interest as promising carbon materials since they were discovered in 2004.[1] Recently, many efforts are focused on their prospective applications in optoelectronic devices,[2] photocatalysis,[3] electrocatalysis,[4] biosensing, and bioimaging,[5-7] owing to their superior properties such as bright luminescence, good biocompatibility, and low toxicity.[8, 9] Specifically, their potential applications in biological field are highly desired. Therefore, intensive investigations are carried out and numerous synthetic methods are developed,[10-12] such as electrochemical oxidation,[13] ultrasonic treatment,[14] microwave methods,[15] solid thermal treatment,[16] and hydrothermal method[17].

Now, CQDs have broad applications in biochemical assays. Chen et al. synthesized CQDs from oil acid for cell imaging.[18] Zhang's group fabricated CQDs via the oxidation of activated carbon by nitric acid. They also demonstrated selective and sensitive responses of CQDs to Cu^{2+}.[19] However, un-doped CQDs might have the disadvantage of self-quenching, thereby limiting their further applications in bioanalysis.[20] This is due to the intra-molecular ground-state dimmer complex or energy transfer between the adjacent CQDs,

Alternatively, doped CQDs can almost remain all the advantages of blank CQDs and further avoid self-quenching phenomenon because of their substantial ensemble Stokes shift. Therefore, many researchers pay much attention to doped CQDs with heteroatoms, especially nitrogen and sulfur.[21-23] Our group synthesized N-doped

CQDs (N-CQDs) by thermal route from streptomycin for cell imaging.[24] We also developed a solvent-free synthesis method to prepare SN-CQDs from glutathione for highly selective and sensitive detection for mercury (II) ions.[25] It needs to emphasize that graphitic carbon nitride quantum dots (GNCQDs) are unique among heteroatom doped CQDs for their similar structures to graphene. They have broad applications in biomass conversion and sustainable chemistry, due to their functional groups.[26,16,27]

Mercury(II) ions (Hg^{2+}) is one of heavy metal ions widely used in industrial and agriculture.[28] Its strong toxicity and bioaccumulation result in serious human health problem even at a very low level.[29] Therefore, developing novel method for trace detection of Hg^{2+} is very important. Conventional analytical approaches include atomic absorption/emission spectroscopy,[30, 31] Auger-electron spectroscopy,[32] inductively coupled plasma mass spectrometry,[33] ultraviolet-visible spectrometry,[34] and polarography[35].

In this work, we developed a facile one-step route for synthesis of OS-GNCQDs from citric acid and thiourea (Scheme 1). The optical properties of the as-prepared OS-GNCQDs were examined in details. Furthermore, OS-GNCQDs were explored for selective and sensitive detection of Hg^{2+} as a model system.

Experimental

Materials

Citric acid and thiourea were purchased from Sinopharm Chemical Reagent Co., Ltd. (Shanghai, China). Mercuric nitrate, sodium nitrate, zinc sulfate heptahydrate, silver

nitrate, manganese acetate tetrahydrate, copper nitrate trihydrate, nickel chloride hexahydrate, magnesium sulfate anhydrous, barium nitrate, aluminum nitrate nonahydrate, calcium nitrate tetrahydrate, cadmium chloride hemi(pentahydrate), ferric chloride, potassium chloride, iron(Ⅱ) chloride tetrahydrate, and lead nitrate were received from Aladdin Chemistry Reagent Company (Shanghai, China). All the other chemicals were analytical grade and used as received. Twice-distilled water was used throughout the whole experiments.

Preparation of OS-GNCQDs

For typical preparation of OS-GNCQDs (Scheme 1), 0.21 g citric acid and 0.23 g thiourea were mixed together under stirring (Fig. S1, Supporting Information). Next, the mixture was put into a 50 ml Teflon-lined autoclave, heated at 200 °C for 2.0 h (Fig. S2, Supporting Information), and cooled to room temperature in air. The product was dissolved with water, and re-purified with a 0.22 μm filter membrane to discard the nonfluorescent deposits, which were some large particles with flake-like structure. (Fig. S3, Supporting Information). The supernatant was collected and further diluted to prepare OS-GNCQDs suspensions (5.0 mg mL^{-1}).

Instruments

UV-vis absorption spectra of the samples were recorded on a Lambda 950 UV-vis spectrophotometer (Perkin-Elmer, USA). Fluorescence emission spectroscopy was carried out on a LS-45 fluorescence spectrophotometer (Perkin-Elmer, UK). X-ray

diffraction (XRD) measurements were performed on a Philips PW3040/60 automatic powder diffractometer using Cu Kα radiation. Fourier transform infrared spectra (FT-IR) were recorded on a Nicolet 670 FT-IR spectrometer in the form of KBr pellets. Transmission electron microscopy (TEM) and high resolution TEM (HR-TEM) images were taken on a JEOL-2100F transmission electron microscope. X-ray photoelectron spectra (XPS) were acquired on a Themo SCIENTIFIC ESCALAB 250 spectrometer with Al Kα X-ray radiation (1486.6 eV).

Fluorescence detection of Hg^{2+}

For a typical assay, 5.0 μL of OS-GNCQDs suspension (5.0 mg mL^{-1}) was diluted with 3.0 mL of water, followed by the addition of different concentrations of Hg^{2+}. The mixed solutions were remained static, reacted for 20 min, and finally recorded the associated fluorescence quenching spectra with the excitation wavelength of 369 nm at room temperature.

Selectivity and interference measurements

The selectivity of OS-GNCQDs was examined by some interfering compounds such as Ag^{+}, Al^{3+}, Cd^{2+}, Co^{2+}, Cu^{2+}, Fe^{2+}, Fe^{3+}, Mg^{2+}, Mn^{2+}, Na^{+}, Ni^{2+}, Pb^{2+}, and Zn^{2+} under the identical conditions. The concentrations of Hg^{2+} and the interferent ions were all 50.0 μM. For studying the interference, the OS-GNCQDs suspension was mixed with Hg^{2+} in the absence and presence of other interferent chemicals with the concentration of four times as that of Hg^{2+}. The associated fluorescence spectra were quickly

recorded after incubation of 20 min.

Cell imaging and toxicity assay

The cytotoxicity of OS-GNCQDs to Human Umbilical Vein Endothelial Cells (HUVEC) was evaluated by a standard methylthiazolydiphenyltetrazolium bromide (MTT) assay. HUVEC were seeded in 96-well U-bottom plates at a density of 5.0×10^4 ~1.0×10^5 cells per milliliter (90.0 μL per well) that were initially cultured for 12 h in an incubator (37 °C, 5% CO_2), followed by the addition of the OS-GNCQDs suspension with different concentrations. After another 24 h cultured with OS-GNCQDs, 20.0 μL of the MTT solution (normal saline or 1.0 mg mL^{-1} phosphate buffer solution) was added to each sample, and incubated at 37 °C for 4 h. The culture media were discarded, followed by the addition of 150.0 μL dimethylsulfoxide (DMSO) to dissolve the formazan under shaking for more than 15 min. The corresponding spectra were recorded with a microplate reader at 570 nm. The cell viability rate (*VR*) was calculated based on the below equation:

$$VR\ (\%) = A/A_0 \times 100\%$$

where A is the absorbance of the experimental group (the cells were treated with the OS-GNCQDs suspensions) and A_0 is the absorbance of the control group.

Results and discussion

Fig. 1 shows the optical properties of OS-GNCQDs. Specifically, there is a UV-vis absorption peak centered at 338 nm, implying the presence of carbonyl or conjugated carbonyl groups. At the same time, the excitation and emission peaks are emerged at

369 and 444 nm, respectively. In addition, the OS-GNCQDs suspension exhibits yellow under visible light, while it is blue upon excitation with UV light of 365 nm (insets in Fig. 1A), respectively.

As illustrated in Fig. 1B, the fluorescence spectra of OS-GNCQDs shift positively by adjusting the excitation wavelength from 369 to 415 nm, accompanied with the fast decrease of the PL intensities. It indicates the excitation-dependent emission behavior of OS-GNCQDs, as supported by the previous report.[7, 18] Meanwhile, using quinine sulfate (54% in 0.1 mol/L H_2SO_4, λ_{ex} = 369 nm) as a reference, the fluorescence quantum yield was calculated to be about 14.5% for OS-GNCQDs. This value is comparable to CQDs prepared from Bombyx mori silk,[36] soya bean grounds,[37] and ionic liquids,[38] which was also identical to previous research where heteroatoms doped CQDs can enhance fluorescence dramatically.[20, 39]

As shown by TEM images (Fig. 2), OS-GNCQDs have spherical shapes with the average size of 2.78 nm, which is similar to the previous work.[3] Furthermore, well-defined lattice fringes are clearly observed (inset in Fig. 2A), with an inter-fringe distance of 0.202 nm, corresponding to the (102) diffraction planes of graphitic (sp^2) carbon.[40] This value is matched well with CQDs using pemelo peel[40] and natural gas soot[41] as carbon sources. Fig. 2B reveals the narrow size distribution of OS-GNCQDs, with the average size of 2.75 nm.

As displayed in Fig. 3A, there is a broad peak located at 27.0º and a weak one at 13.4º in the XRD pattern of OS-GNCQDs. The former represents the interplaner graphitic stacking, and the latter is indicative of in-planer structural packing,

reflecting the formation of graphitic carbon nitride.[42, 43]

Meanwhile, FT-IR analysis was carried out to characterize the surface groups of OS-GNCQDs (Fig. 3B). The peaks emerged at 3415 and 3175 cm^{-1} correspond to the stretching modes of N-H/O-H, suggesting highly hydrophilic property of OS-GNCQDs.[3] The peak of 2380 cm^{-1} is ascribed to the stretching vibration of S-H group, 2070 cm^{-1} to C–N group,[23] 1670 cm^{-1} to the vibration absorption of C=O in COOH, 1410 cm^{-1} to COO^- group, and 1180~1080 cm^{-1} to C=S vibrations.[3, 23] These results illustrate OS-GNCQDs with desirable functional groups.

As revealed by survey XPS spectrum of NSCDs (Fig. 4A), the typical product mainly contains O_{1s}, N_{1s}, C_{1s}, S_{2s}, and S_{2p} elements. Specifically, the high-resolution C_{1s} spectrum (Fig. 4B) shows five peaks detected at 284.2, 284.7, 285.3, 287.7, and 288.6 eV, which are attributed to C=C, C-C/C-H, C-OH/C-O-C, C=O, and COOH groups, respectively.[44] And there are two peaks located at 398.9 and 399.6 eV in the high-resolution N_{1s} region (Fig. 4C), which is come from pyridinic N and pyrrolic N,[11] respectively. Similarly, two peaks are emerged at 530.8 and 531.7 eV for the O_{1s} spectrum (Fig. S4, , Supporting Information), which are originated from C-O and C=O bands,[45] respectively. Additionally, seven peaks are detected in the S_{2p} spectrum (Fig. 4D), corresponding to –SH (161.8 eV), C-Sn-C (n=1 or 2, 163.5 eV), -C=S- (164.8 eV), sulfoxide (166.2 eV), and -C-SOx- (x=2, 167.7 eV; 3, 168.5 eV; 4, 169.3 eV),[23, 46] respectively. These phenomena demonstrate the formation of OS-GNCQDs in the present work.

Fig. S5 (Supporting Information) illustrates the effects of pH values and salinity

in the solution on the PL intensities of OS-GNCQDs. The results verify good stability of OS-GNCQDs in different physiological environment. Besides, OS-GNCQDs exhibit better photostability than the traditional organic dyes such as rhodamine 6G. After three months storage at room temperature, OS-GNCQDs remain similar PL intensity. These properties make OS-GNCQDs a potential fluorescent probe for biosensing and bioimaging.

To estimate the selectivity of OS-GNCQDs as a fluorescent probe, the PL intensities of OS-GNCQDs were analyzed in the presence of metal ions at the concentration of 50.0 μM (Fig. 5A). It is found that fluorescence responses of OS-GNCQDs are different in the presence of different metal ions even under the same conditions. Impressively, the PL intensity of OS-GNCQDs can be greatly quenched in the case of Hg^{2+}. Based on this phenomenon, OS-GNCQDs were efficiently used for selective detection of Hg^{2+} in the coexistence of other metal ions at the concentration of 200.0 μM (Fig. 5B). The outstanding selectivity and specificity can be ascribed to strong affinity of Hg^{2+} to amino groups and thiourea groups on the surface of OS-GNCQDs than other metal ions.

Fig. 6 shows the changes of high-resolution N and S spectra of OS-GNCQDs before and after the addition of Hg^{2+}. The peak of N_{1s} at 399.0 eV greatly decreases (Fig. 6A). It clearly demonstrates that Hg^{2+} has high interactions with the pridine nitrogen in OS-GNCQDs, which generate energy transfer from OS-GNCQDs to Hg^{2+}, leading to the fluorescence quenching. Moreover, the peak of sulfur at 162.6 eV significantly increases and the peak at 168.0 eV obviously decreases (Fig. 6B). It is

ascribed to formation of –C=S-Hg complexes based on high affinity of thiourea groups to Hg^{2+}. The as-formed complexes can facilitate electron transfer and restrain the radioactive recombination of excitations, leading to remarkable quenching effects on fluorescence intensity.[47]

In addition, the PL lifetime of OS-GNCQDs is measured to be 7.88 ns, with the excitation and emission wavelengths of 369 and 444 nm, respectively (Fig. 7). Nevertheless, the respective lifetime is decreased to 7.70 ns after the addition of Hg^{2+}, mainly due to static quenching occurred in this case. Furthermore, this value is equal to that of CQDs prepared from streptomycin.[24] It means that OS-GNCQDs can be used as a promise probe in biological analysis.

As described in Fig. 8, the PL intensities of OS-GNCQDs linearly decrease with Hg^{2+} concentrations. The quenching efficiency can be well fitted by the following Stern-Volmer equation:

$$F_0/F=1+K_{sv}Q,$$

where F_0 and F are the PL intensities of OS-GNCQDs in the absence and presence of Hg^{2+}, respectively, Q is the concentration of Hg^{2+}, and K_{sv} is the Stern-Volmer constant.

Specifically, the PL intensities show linear responses to Hg^{2+} concentrations in the range of 0.001~0.5 μM (inset in Fig. 8). The detection limit is about 0.37 nM (S/N = 3) for Hg^{2+} detection. OS-GNCQDs have good sensitivity and wide linear range, in contrast to those in literature, as listed in Table S1 (Supporting Information). The superior selectivity and sensitivity make OS-GNCQDs as a promising fluorescent

probe in biomedical and environmental systems.

The MTT assay was conducted with HUVEC as a model cell to test the cytotoxicity of OS-GNCQDs, since cancer cells usually have more resistance to most of chemical compounds. As depicted in Fig. 9, OS-GNCQDs exhibit good biocompatibility and low cytotoxicity for HUVEC, revealing the possible application of OS-GNCQDs for cell imaging.

Fig. 10 shows the confocal images of HeLa cells treated with OS-GNCQDs (75.0 μg mL^{-1}). The fluorescence becomes brighter with the increase of the CQDs concentrations, and vise versa (Fig. S6, Supporting Information). It is noteworthy that the concentration of OS-GNCQDs (75.0 μg mL^{-1}) is much higher and the incubation time (24 h) is much longer for in vitro evaluation. These results indicate the better biocompatibility of OS-GNCQDs which can be used for in vivo applications such as bioimaging.

Before incubation of HeLa cells with OS-GNCQDs solution, there is no fluorescent response at the wavelength of 488 nm (Fig. 10A and B). After the incubation, the cells become bright green in cytoplasm under the excitation of 488 nm. It means that CQDs can be easily penetrated into cytoplasm and labeled them simultaneously, illustrating the greatly improved fluorescence performance of OS-GNCQDs as fluorescent probe in bioimaging.[24, 43, 44] Therefore, OS-GNCQDs can be applied for potentially investigation of label cytoplasm.

Conclusion

In summary, we have reported a simple route for synthesis of water-soluble OS-GNCQDs by thermal treatment of citric acid and thiourea. The as-prepared uniform OS-GNCQDs possess a quantum yield of 14.5%, and have the average size of 2.78 nm, which is used for selective and sensitive detection of Hg^{2+} with the detection limit of 0.37 nM. Furthermore, OS-GNCQDs were explored for bioimaging with improved biocompatibility.

Acknowledgments

This work was financially supported by National Natural Science Foundation of China (Nos. 21475118, 21175118, 21275130, 21305128 and 21345006), and Zhejiang province university young academic leaders of academic climbing project (No. pd2013055).

References

1. X. Xu, R. Ray, Y. Gu, H. J. Ploehn, L. Gearheart, K. Raker and W. A. Scrivens, *J. Am. Chem. Soc.*, 2004, **126**, 12736-12737.
2. D. Zhang, Y. Hao, L. Zheng, Y. Ma, H. Feng and H. Luo, *J. Mater. Chem. A*, 2013, **1**, 7584-7591.
3. D. Qu, M. Zheng, P. Du, L. Zhang, Y. Zhou, D. Li, H. Tan, Z. Zhao, Z. Xie and Z. Sun, *Nanoscale*, 2013, **5**, 12272-12277.
4. Z. Liu, H. Nie, Z. Yang, J. Zhang, Z. Jin, Y. Lu, Z. Xiao and S. Huang, *Nanoscale*,

2013, **5**, 3283-3288.

5. K. Qu, J. Wang, J. Ren and X. Qu, *Chem. Eur. J.*, 2013, **19**, 7243-7249.
6. A. Salinas-Castillo, M. Ariza-Avidad, C. Pritz, M. Camprubi-Robles, B. Fernandez, M. J. Ruedas-Rama, A. Megia-Fernandez, A. Lapresta-Fernandez, F. Santoyo-Gonzalez, A. Schrott-Fischer and L. F. Capitan-Vallvey, *Chem. Commun.*, 2013, **49**, 1103-1105.
7. L. Shen, L. Zhang, M. Chen, X. Chen and J. Wang, *Carbon*, 2013, **55**, 343-349.
8. J. C. G. Esteves da Silva and H. M. R. Gonçalves, *Trends Anal. Chem.*, 2011, **30**, 1327-1336.
9. P. G. Luo, S. Sahu, S.-T. Yang, S. K. Sonkar, J. Wang, H. Wang, G. E. LeCroy, L. Cao and Y.-P. Sun, *J. Mater. Chem. B*, 2013, **1**, 2116-2127.
10. M. Tan, L. Zhang, R. Tang, X. Song, Y. Li, H. Wu, Y. Wang, G. Lv, W. Liu and X. Ma, *Talanta*, 2013, **115**, 950-956.
11. Z. Qian, J. Ma, X. Shan, L. Shao, J. Zhou, J. Chen and H. Feng, *RSC Adv.*, 2013, **3**, 14571-14579.
12. X. Wang, K. Qu, B. Xu, J. Ren and X. Qu, *Nano Res.*, 2011, **4**, 908-920.
13. Y.-L. Zhang, L. Wang, H.-C. Zhang, Y. Liu, H.-Y. Wang, Z.-H. Kang and S.-T. Lee, *RSC Adv.*, 2013, **3**, 3733-3738.
14. S. Zhuo, M. Shao and S.-T. Lee, *ACS Nano*, 2012, **6**, 1059-1064.
15. Y. Liu, N. Xiao, N. Gong, H. Wang, X. Shi, W. Gu and L. Ye, *Carbon*, 2014, **68**, 258-264.
16. J. Zhou, Y. Yang and C.-Y. Zhang, *Chem. Commun.*, 2013, **49**, 8605-8607.

17. W. Li, Z. Zhang, B. Kong, S. Feng, J. Wang, L. Wang, J. Yang, F. Zhang, P. Wu and D. Zhao, *Angew. Chem. Int. Ed.*, 2013, **52**, 1-6.

18. B. Chen, F. Li, S. Li, W. Weng, H. Guo, T. Guo, X. Zhang, Y. Chen, T. Huang, X. Hong, S. You, Y. Lin, K. Zeng and S. Chen, *Nanoscale*, 2013, **5**, 1967-1971.

19. S. Zhang, Q. Wang, G. Tian and H. Ge, *Mater. Lett.*, 2014, **115**, 233-236.

20. P. Wu and X.-P. Yan, *Chem. Soc. Rev.*, 2013, **42**, 5489-5521.

21. W. Shi, X. Li and H. Ma, *Angew. Chem.*, 2012, **124**, 6538-6541.

22. S. Chandra, P. Patra, S. H. Pathan, S. Roy, S. Mitra, A. Layek, R. Bhar, P. Pramanik and A. Goswami, *J. Mater. Chem. B*, 2013, **1**, 2375-2382.

23. D. Sun, R. Ban, P.-H. Zhang, G.-H. Wu, J.-R. Zhang and J.-J. Zhu, *Carbon*, 2013, **64**, 424-434.

24. W. Wang, Y.-C. Lu, H. Huang, J.-J. Feng, J.-R. Chen and A.-J. Wang, *Analyst*, 2014, **139**, 1692-1696.

25. W. Wang, Y.-C. Lu, H. Huang, A.-J. Wang, J.-R. Chen and J.-J. Feng, *Sensors Actuators B: Chem.*, 2014, **202**, 741-747.

26. Y. Wang, X. Wang and M. Antonietti, *Angew. Chem. Int. Ed.*, 2012, **51**, 68-89.

27. Y. Zhang, J. Liu, G. Wu and W. Chen, *Nanoscale*, 2012, **4**, 5300-5303.

28. R. Liu, H. Li, W. Kong, J. Liu, Y. Liu, C. Tong, X. Zhang and Z. Kang, *Mater. Res. Bull.*, 2013, **48**, 2529-2534.

29. R. Zhang and W. Chen, *Biosens. Bioelectron.*, 2014, **55**, 83-90.

30. J. Margetínová, P. Houserová-Pelcová and V. Kubáň, *Anal. Chim. Acta*, 2008, **615**, 115-123.

31. S. Gil, I. Lavilla and C. Bendicho, *Spectrochim. Acta B*, 2007, **62**, 69-75.

32. M. Miró and E. H. Hansen, *Anal. Chim. Acta*, 2013, **782**, 1-11.

33. A. Castillo, A. F. Roig-Navarro and O. J. Pozo, *Anal. Chim. Acta*, 2006, **577**, 18-25.

34. H. Bagheri and A. Gholami, *Talanta*, 2001, **55**, 1141-1150.

35. S. Z. Milić, N. I. Potkonjak, S. Ž. Gorjanović, S. D. Veljović-Jovanović, F. T. Pastor and D. Ž. Sužnjević, *Electroanal.*, 2011, **23**, 2935-2940.

36. Z. L. Wu, P. Zhang, M. X. Gao, C. F. Liu, W. Wang, F. Leng and C. Z. Huang, *J. Mater. Chem. B*, 2013, **1**, 2868-2873.

37. W. Li, Z. Yue, C. Wang, W. Zhang and G. Liu, *RSC Adv.*, 2013, **3**, 20662-20665.

38. A. Zhao, C. Zhao, M. Li, J. Ren and X. Qu, *Anal. Chim. Acta*, 2014, **809**, 128-133.

39. C. Liu, P. Zhang, F. Tian, W. Li, F. Li and W. Liu, *J. Mater. Chem.*, 2011, **21**, 13163-13167.

40. W. Lu, X. Qin, S. Liu, G. Chang, Y. Zhang, Y. Luo, A. M. Asiri, A. O. Al-Youbi and X. Sun, *Anal. Chem.*, 2012, **84**, 5351-5357.

41. L. Tian, D. Ghosh, W. Chen, S. Pradhan, X. Chang and S. Chen, *Chem. Mater.*, 2009, **21**, 2803-2809.

42. Q. Su, J. Sun, J. Wang, Z. Yang, W. Cheng and S. Zhang, *Catalysis Science & Technology*, 2014, **4**, 1556-1562.

43. G. Zhang, J. Zhang, M. Zhang and X. Wang, *J. Mater. Chem.*, 2012, **22**, 8083-8091.

44. S. Sahu, B. Behera, T. K. Maiti and S. Mohapatra, *Chem. Commun.*, 2012, **48**, 8835-8837.

45.J. Wei, J. Shen, X. Zhang, S. Guo, J. Pan, X. Hou, H. Zhang, L. Wang and B. Feng, *RSC Adv.*, 2013, **3**, 13119-13122.

46. Y. Su, Y. Zhang, X. Zhuang, S. Li, D. Wu, F. Zhang and X. Feng, *Carbon*, 2013, **62**, 296-301.

47. H. Huang, J.-J. Lv, D.-L. Zhou, N. Bao, Y. Xu, A.-J. Wang and J.-J. Feng, *RSC Adv.*, 2013, **3**, 21691-21696.

Captions

Scheme 1 Formation mechanism of highly fluorescent OS-GNCQDs.

Fig. 1 (A) Absorbance, excitation, and emission spectra of OS-GNCQDs. (B) The excitation-dependent emission spectra of OS-GNCQDs. Insets show the corresponding photographs taken under visible light (left) and UV light of 365 nm (right).

Fig. 2 TEM image (A) and the respective size distribution (B) measured by 400 nanodots randomly. Inset shows high-resolution TEM image of an individual nanodot.

Fig. 3 XRD pattern (A) and FT-IR spectrum (B) of OS-GNCQDs.

Fig. 4 Survey (A), high-resolution C_{1s} (B), N_{1s} (C), and S_{2p} (D) XPS spectra of OS-GNCQDs.

Fig. 5 (A) Fluorescence responses of OS-GNCQDs in the presence of different metal ions (λ_{ex} = 369 nm; $[M^{n+}]$ = 50.0 μM). Inset displays the photographs in accordance with the spectra. (B) The relative fluorescence intensities (F/F_0) of OS-GCNQDs in the presence of metal ions (200.0 μM), and treat the mixture solution with 50.0 μM Hg^{2+} in red column.

Fig. 6 High-resolution N_{1s} (A) and S_{2p} (B) XPS spectra of OS-GCNQDs before (a) and after (b) the addition of Hg^{2+}.

Fig. 7 Fluorescence decay trace of OS-GCNQDs upon excitation at 369 nm.

Fig. 8 The relationship of the F/F_0 and Hg^{2+} concentrations. Inset shows the linear range of 0.001~0.5 μM. The error bars represent variations among three independent measurements.

Fig. 9 Cell viability assays of HUVEC treated with different concentrations of OS-GNCQDs.

Fig. 10 Images of Hela cells in the absence (A, B) and presence (C, D) of OS-GNCQDs taken under bright field (A, C) and at excitation wavelength of 488 nm (B, D) with 75.0 μg mL^{-1} of OS-GNCQDs.

Figures

Scheme 1

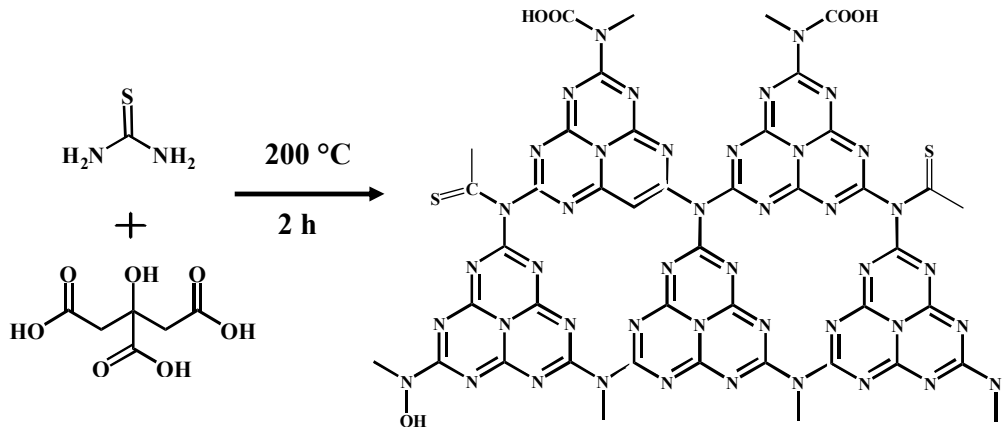

Fig. 1

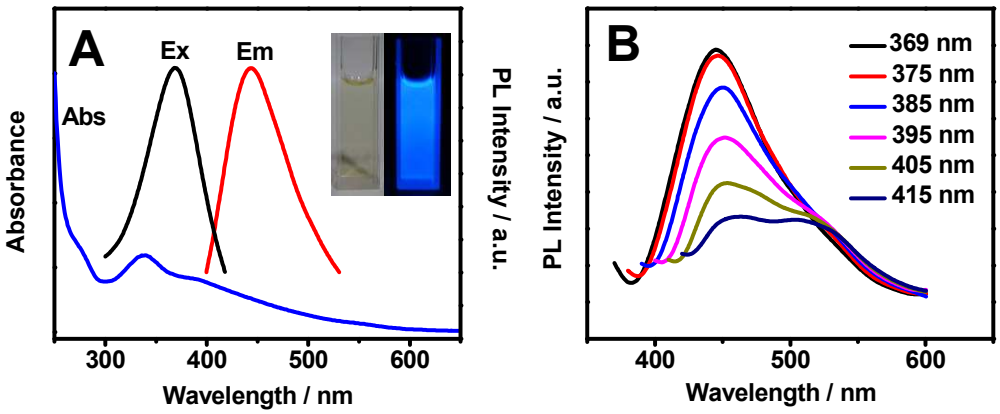

Fig. 2

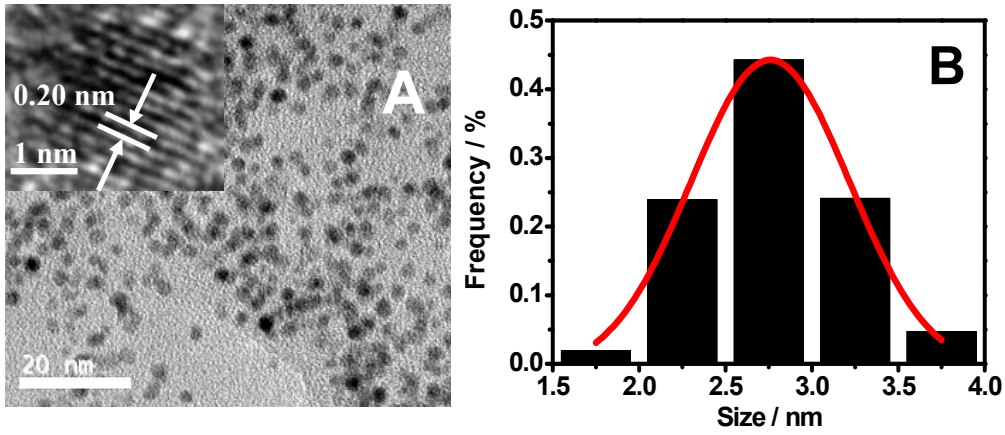

Fig. 3

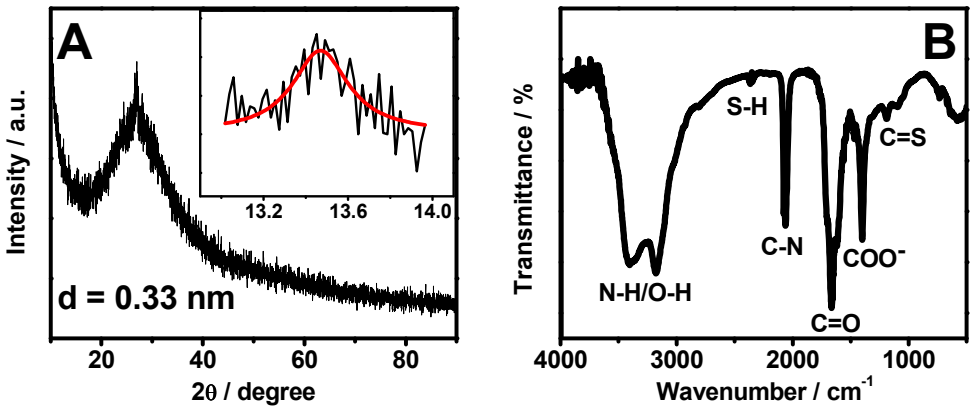

Fig. 4

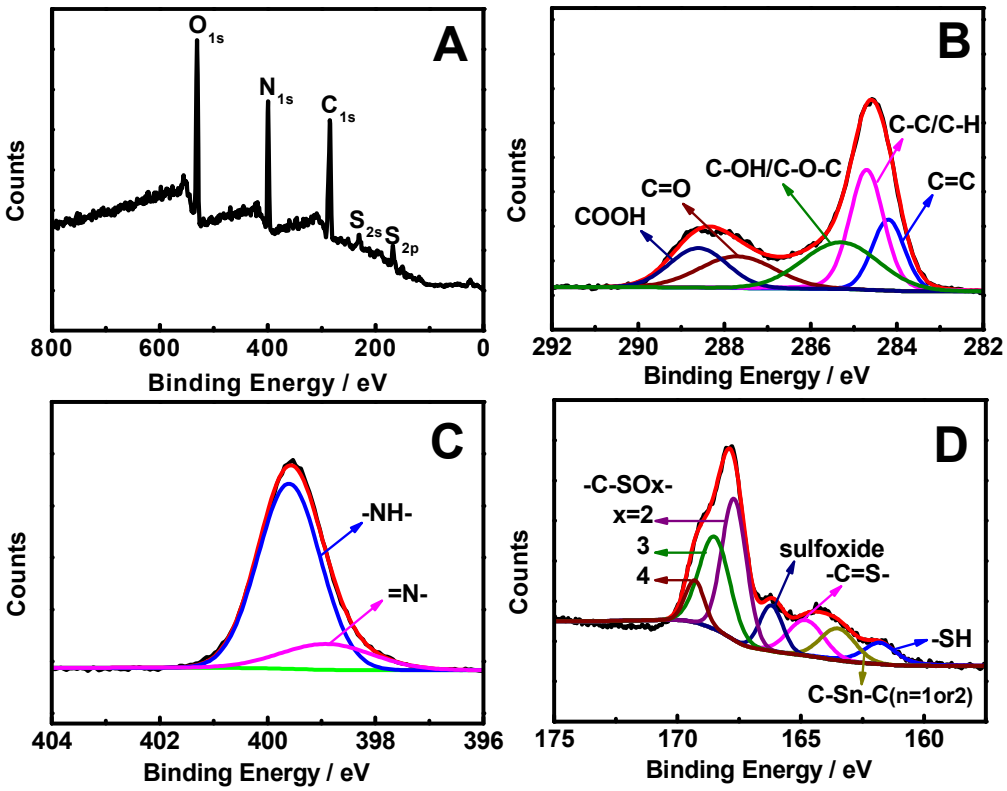

Fig. 5

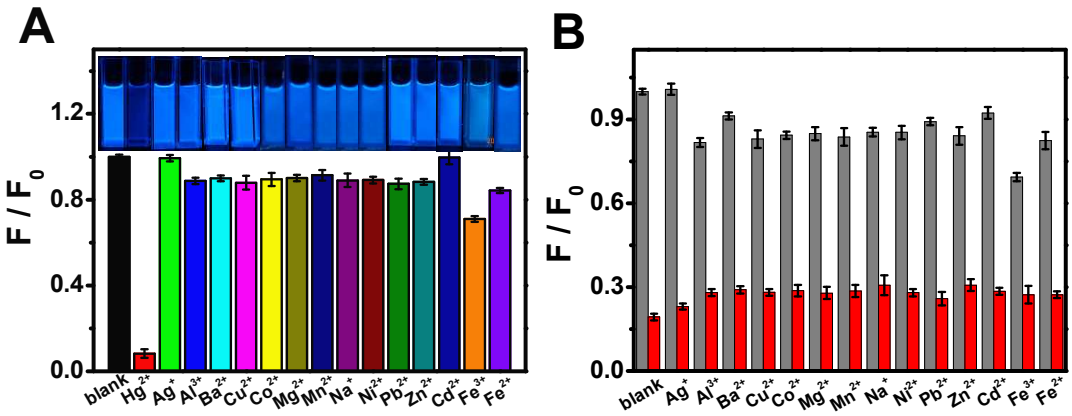

Fig. 6

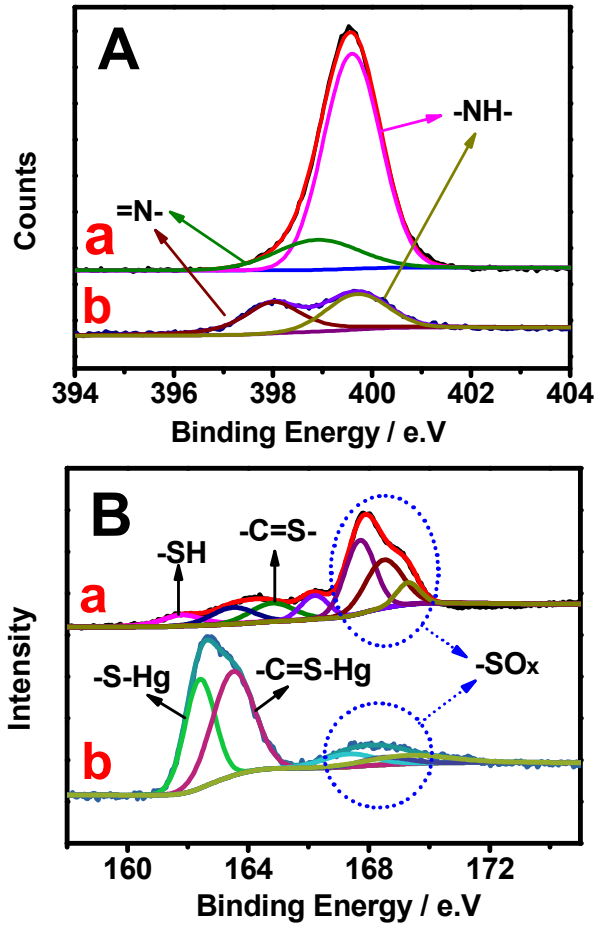

Fig. 7

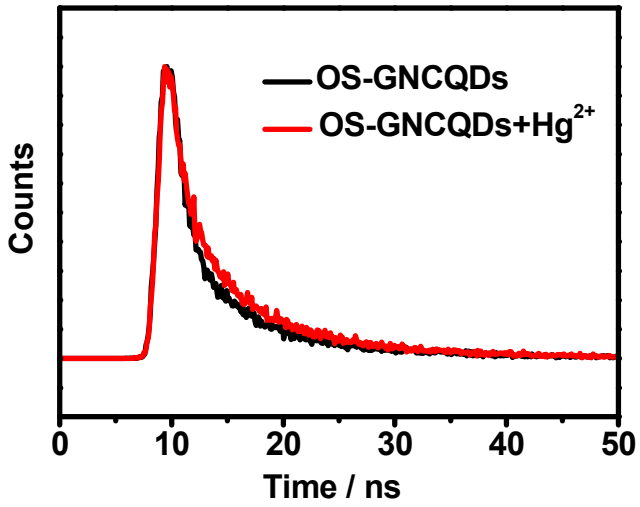

Fig. 8

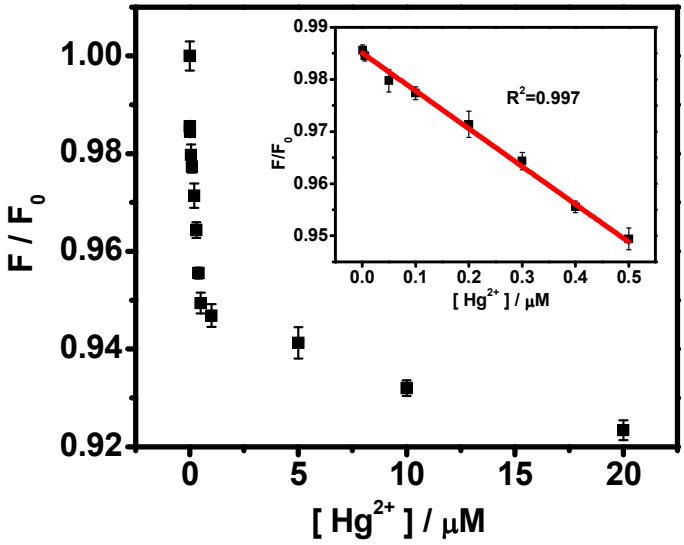

Fig. 9

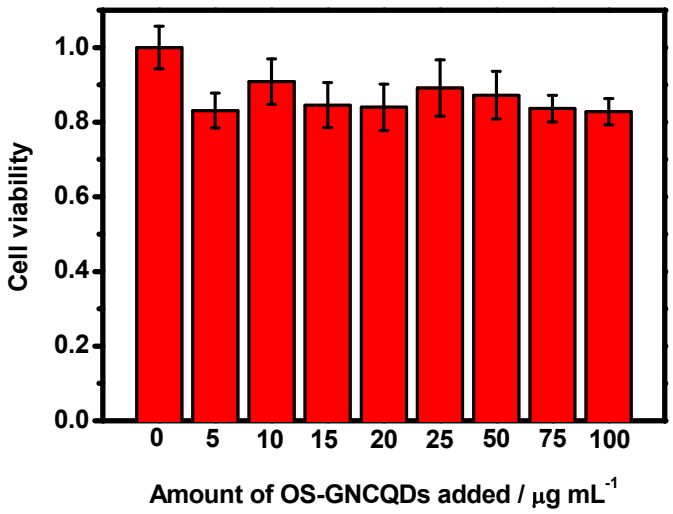

Fig. 10